CHEMISTRY OF MATERIALS

Article

pubs.acs.org/cm

# Lithiation Behavior of Silicon-Rich Oxide ($SiO_{1/3}$): A First-Principles Study

Chia-Yun Chou[†] and Gyeong S. Hwang*[,†,‡]

[†]Materials Science and Engineering Program and [‡]Department of Chemical Engineering, University of Texas at Austin, Austin, Texas 78712, United States

**ABSTRACT:** Silicon suboxides ($SiO_x$, $x < 2$) have been recognized as a promising anode material for high-performance Li-ion batteries (LIBs), especially when the O content is relatively low. To better understand the lithiation behavior in partially oxidized silicon at the atomistic level, we perform density functional theory calculations to examine the structural evolution, bonding mechanism, mechanical property, and voltage profile of lithiated $a$-$SiO_{1/3}$. With lithiation, the $a$-$SiO_{1/3}$ host matrix gradually disintegrates as Li atoms are accommodated by both Si and O atoms. Interestingly, we find that the Si−Li coordination number (CN) monotonically increases up to $CN_{Si-Li} \approx 10$ in $a$-$Li_4SiO_{1/3}$, whereas $CN_{O-Li}$ tends to saturate far before full lithiation at $CN_{O-Li} \approx 6$; the formation mechanism of such intriguing $Li_6O$ complexes with $O_h$ symmetry is investigated via detailed electronic structure analyses. Li incorporation in the $a$-$SiO_{1/3}$ matrix is predicted to be highly favorable with a capacity comparable to that of fully lithiated Si (Li:Si ratio ≈ 4); additionally, the approximated lithiation voltage between 0.2 and 0.8 V is also well within the desirable range for LIB anode applications. Our study highlights the importance of controlling the Si:O ratio as well as O spatial distribution in order to tailor the desired lithiation properties; such a realization may benefit the rational design and development of high-performance silicon suboxide based anodes via fine-tuning of the oxidation conditions.

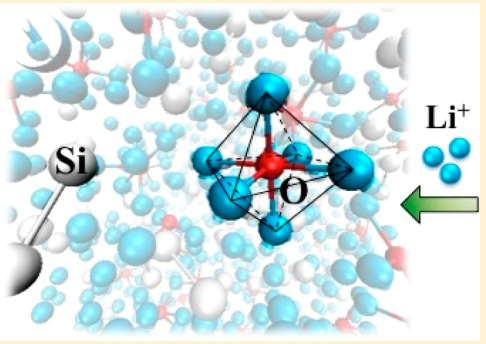


**KEYWORDS:** *silicon suboxide, lithiation, $Li_6O$ polycation, LIB anode, density functional theory*

## 1. INTRODUCTION

Silicon (Si) has recently emerged as an attractive material in replacing the carbon-based anodes for Li-ion batteries (LIBs) because of its impressive theoretical capacity.[1−5] However, the practical use of silicon as an anode material is hampered mainly by a severe volume change (>300%) during cycling, which causes pulverization, loss of electrical contact, and consequently early capacity fading. Considerable efforts have been made to overcome this drawback, including alloying silicon with active/inactive elements,[6−8] structural modifications such as utilizing nanoparticles and nanowires,[9−11] and combing silicon with carbonaceous materials to form silicon/carbon or silicon/graphene composites.[12−19]

Silicon suboxides $SiO_x$ ($x < 2$) have also been considered as a potential LIB anode.[20−31] It was suggested that such silicon suboxides may form silicon nanocrystallites dispersed in the $a$-$SiO_2$ matrix,[32−36] leading to active/inactive structures that help buffer the strain during cycling and hence much improved reversible capacities. Recently, researchers have been toying with the idea of controlled oxidation, in which $a$-$SiO_x$ of different O contents ($x$ mainly lower than 0.5) have been tested to evaluate the effect of oxidation on the anode performance. Kim et al. recommended that the O concentration should be reduced below 18 atom % in order to increase the initial capacity,[30] and Abel et al. later demonstrated that nanostructured silicon thin films with homogeneous O incorporation (≈13 atom % O) in combination with surface oxidation were able to deliver an excellent capacity (≈2200 mAh/g) with nearly no capacity loss for the first 120 cycles, and 80% of the initial reversible capacity was retained after 300 cycles.[31] Despite these encouraging improvements, the fundamental understanding regarding the nature and properties of lithiated $a$-$SiO_x$ of relatively low O contents ($x \leq 0.5$) is still limited; to the best of our knowledge, no atomistic study has been reported regarding the lithiation behavior in the suboxide materials.

In this paper, on the basis of density functional theory (DFT) calculations, we present the structural evolution and voltage profile of the lithiated $a$-$SiO_{1/3}$ and also discuss the bonding mechanism of the unique oxygen complex formation during lithiation.

## 2. COMPUTATIONAL METHOD

The model structures of $a$-$Li_xSiO_{1/3}$ alloys were created using ab initio molecular dynamics (AIMD) simulations based on the atomic configurations of $a$-$Li_xSi$ alloys that were previously obtained using the combined modified embedded atom method and AIMD simulations (see refs 37 and 38 for detailed computational methods). According to the previous study, Li and Si atoms are overall well mixed

**Received:** April 20, 2013
**Revised:** July 30, 2013
**Published:** August 2, 2013

 © 2013 American Chemical Society 

with no segregation in the bulk $a$-$Li_xSi$ alloy,[38] which is therefore likely a good starting configuration for the $a$-$Li_xSiO_{1/3}$ structures (where constituent atoms are also found to be well dispersed as discussed later). The $a$-$Li_xSiO_{1/3}$ alloys of interest were annealed at 1500 K for 2 ps with a time step of 1 fs to allow facile local structure rearrangements and then rapidly quenched to 300 K at a rate of 0.6 K/fs, along with geometric optimization. Here, the temperature was controlled via a Nose-Hover thermostat. The $a$-$Li_xSiO_{1/3}$ structures considered are summarized in Table 1, and three different supercells were constructed

**Table 1. Composition and Volume of the $a$-$Li_xSiO_{1/3}$ Systems Employed in This Work[a]**

| $x$ in $Li_xSiO_{1/3}$ (#Li/Si/O) | volume (Å$^3$) |
|---|---|
| 0.0 (0/24/8) | 568.1 ± 9.0 |
| 0.5 (12/24/8) | 710.1 ± 21.4 |
| 1.0 (24/24/8) | 851.9 ± 13.2 |
| 1.5 (36/24/8) | 1044.3 ± 28.5 |
| 2.0 (48/24/8) | 1177.2 ± 10.8 |
| 2.5 (60/24/8) | 1365.8 ± 32.4 |
| 3.0 (72/24/8) | 1553.6 ± 37.2 |
| 3.5 (84/24/8) | 1753.7 ± 22.6 |
| 4.0 (96/24/8) | 1963.1 ± 14.0 |

[a]For better statistics, three different samples were constructed for each alloy composition.

for each alloy composition. Note that, although thermodynamically silicon suboxides prefer to disproportionate into Si and $SiO_2$ because of the oxidation energy penalty,[39−41] here we assume a random O distribution by forming Si−O−Si units. This should be reasonable because phase separation usually requires high-temperature annealing to facilitate atomic rearrangements;[32−36] hence, we can expect a rather homogeneous O distribution when the O content is sufficiently low, which is consistent with previous experimental observations.[31]

The DFT calculations reported herein were performed within the generalized gradient approximation (GGA-PW91[42]), as implemented in the *Vienna ab Initio Simulation Package*.[43−45] The projector augmented wave (PAW) method with a planewave basis set was employed to describe the interaction between the core and valence electrons. The PAW method is, in principle, an all-electron frozen-core approach that considers exact valence-wave functions. Valence configurations employed are $1s^22s^1$ for Li, $3s^23p^2$ for Si, and $2s^22p^4$ for O. An energy cutoff of 400 eV was applied for planewave expansion of the electronic eigenfunctions. During geometry optimization, all atoms were fully relaxed using the conjugate gradient method until residual forces on constituent atoms become smaller than $5 \times 10^{-2}$ eV/Å. For Brillouin zone sampling, we find that a $2 \times 2 \times 2$ mesh of $k$ points in the Monkhorst−Pack scheme[46] was sufficient for the highly disordered $a$-$Li_xSiO_{1/3}$ system considered.

## 3. RESULTS AND DISCUSSION

**Structural Evolution.** Figure 1 shows a set of amorphous structures from our AIMD simulations to illustrate the structural evolution of $a$-$Li_xSiO_{1/3}$ alloys with varying Li contents from $x = 0$ to 4. With increasing Li contents, the Si network gradually disintegrates into smaller fragments of lower connectivity, while the Si−O−Si units break up and O atoms tend to be surrounded by Li atoms.

To gain more detailed structural information, the $a$-$Li_xSiO_{1/3}$ structures were characterized using atomic pair distribution functions (PDFs). The PDF is defined as[47]

$$g(r) = \frac{N}{V}\frac{n(r)}{4\pi^2\Delta r} \quad (1)$$

where $n(r)$ represents particles in a shell within the region $r \pm \Delta r/2$, where $\Delta r$ is the shell thickness and $N$ denotes the

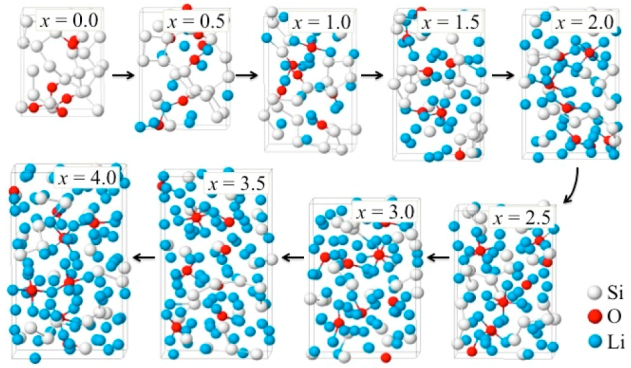


**Figure 1.** Structural evolution for $a$-$Li_xSiO_{1/3}$ with increasing Li contents $x$.

number of particles in the model volume $V$. Figure 2 shows the Si−Si, Si−O, Si−Li, and O−Li PDFs in selected $a$-$Li_xSiO_{1/3}$

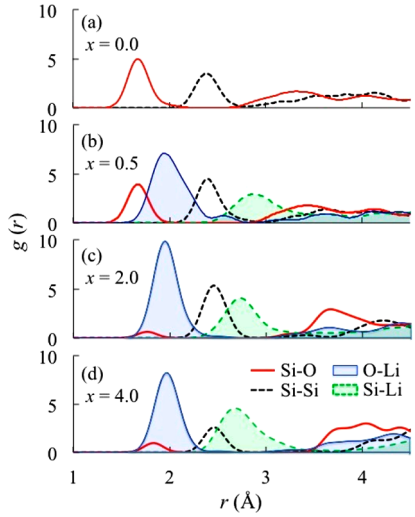


**Figure 2.** Si−Si, Si−O, Si−Li, and O−Li PDFs [$g(r)$] in selected $a$-$Li_xSiO_{1/3}$ alloys ($x$ = 0.0, 0.5, 2.0, and 4.0).

alloys ($x$ = 0, 0.5, 2, and 4); the smooth and broadened $g(r)$ peaks are indicative of the amorphous nature with no long-range order. Looking at the first peak intensities, we find that, with increasing $x$, the Si−Li and especially Li−O peaks become more prominent, while the Si−O and Si−Si peaks dwindle. The reduction in the Si−Si peak intensity is apparently attributed to disintegration of the Si matrix, and similarly the Si−O peak reduction indicates the rupture of Si−O−Si units; this may imply that both Si and O atoms are favorably alloyed with Li atoms.

Figure 3 shows coordination numbers (CNs) calculated by integrating the first peak of $g(r)$ with corresponding cutoff radii. Considering the average Si−Si bond length of ≈2.50 Å in $a$-Si and the Si−Li bond length of ≈2.57−3.09 Å in Li−Si alloys, $r \leq 2.50$ and $r \leq 3.09$ are chosen as the representative cutoff radii for calculating $CN_{Si-Si}$ and $CN_{Si-Li}$, respectively.[38] Likewise, $r \leq 1.86$ (for $CN_{O-Si}$) and $r \leq 2.15$ (for $CN_{O-Li}$) are selected based on the O−Si bond length in $a$-$SiO_2$ and the O−Li bond length in lithium silicates (such as $Li_2Si_2O_5$ and $Li_4SiO_4$).[48−52] As the Li content increases, $CN_{Si-Si}$ and $CN_{O-Si}$ drop from 3.2 and 2.0 (at $x$ = 0) to 0.7 and 0.1 (at $x$ = 4), respectively, because of disintegration of the $a$-$SiO_{1/3}$ host matrix. These low-connectivity Si and isolated O atoms are surrounded by Li


dx.doi.org/10.1021/cm401303n | *Chem. Mater.* 2013, 25, 3435−3440

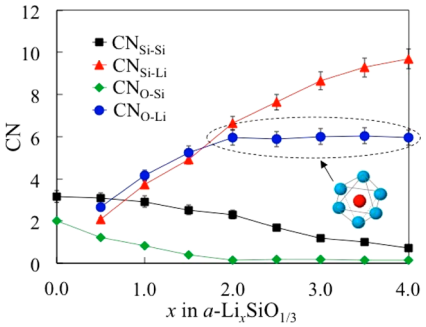


**Figure 3.** Calculated average CNs for Si and O atoms in $a$-$Li_xSiO_{1/3}$ alloys as a function of Li content $x$. The cutoff radii for $CN_{Si-Si}$, $CN_{Si-Li}$, $CN_{O-Si}$, and $CN_{O-Li}$ are 2.50, 3.09, 1.86, and 2.15, respectively.

atoms, as demonstrated by the increasing $CN_{Si-Li}$ and $CN_{O-Li}$ with the Li content $x$. For instance, $CN_{Si-Li}$ gradually increases from 2.1 (at $x = 0.5$) to 9.7 (at $x = 4$), while $CN_{O-Li}$ increases from 2.7 (at $x = 0.5$) to 4.2 (at $x = 1$) and eventually saturates around 6.0 (when $x \geq 2$). It is worth noting the formation of highly symmetric $Li_6O$ complexes with unique $O_h$ symmetry, as illustrated in the inset of Figure 3.

**Bonding Mechanism.** To better understand the interactions between Si, O, and Li atoms, we first calculated their Bader charges[53] in selected $a$-$Li_xSiO_{1/3}$ alloys ($x$ = 0, 0.5, 2, and 4). As summarized in Table 2, the Si charge state varies

**Table 2. Calculated Bader Charges for Si, O, and Li Atoms in Selected $a$-$Li_xSiO_{1/3}$ Alloys**

| | $x = 0$[a] | $x = 0.5$ | $x = 2$ | $x = 4$ |
|---|---|---|---|---|
| Si | 0.04+ (0O)<br>0.76+ (1O)<br>1.52+ (2O)<br>2.10+ (3O) | 0.55+ to 1.58− | 0.16+ to 1.97− | 1.78− to 3.48− |
| O | 1.61− | 1.63− | 1.74− | 1.82− |
| Li | | 0.87+ | 0.84+ | 0.81+, 0.83+[b] |

[a] $n$O in the second column denotes the number of O neighbors. [b] Li in the $Li_6O$ complex.

significantly with changing alloy compositions because Si can donate electrons to O or accept electrons from Li depending on the local atomic environment; this is not surprising given their relative electronegativity values ($\chi_{Li} = 0.98$, $\chi_{Si} = 1.90$, and $\chi_O = 3.44$). In the $a$-$SiO_{1/3}$ matrix, the charge states of Si atoms are estimated to be around 0.0, 0.8+, 1.5+, or 2.1+, depending on the number of O neighbors. As the Li content increases from $x = 0.5$ to 4, the Si charge state varies significantly from 0.6+ to 3.5− depending on the number of neighboring O and Li atoms, while the Li and O charge states remain nearly unchanged (0.8+ to 0.9+ for Li and 1.6− to 1.8− for O). Approaching the fully lithiated phase ($x \geq 4$), each Si atom can accommodate approximately four additional electrons to completely fill the outermost 3s and 3p shells ($3s^23p^6$ Ar-like), whereas each O atom holds two additional electrons to become Ne-like ($2s^22p^6$). Such electron injection with lithiation is apparently responsible for the gradual weakening and disintegration of the $a$-$SiO_{1/3}$ host matrix.

Next we examined the atomic structure and bonding mechanism in fully lithiated $a$-$Li_4SiO_{1/3}$. Each isolated Si anion is surrounded by about 10 Li cations, forming Si-centered polyhedra; similarly, the formation of $Li_{12}Si$ icosahedra has been predicted in the crystalline $Li_{15}Si_4$ structure.[54] On the other hand, as discussed earlier (Figure 3), an isolated O atom tends to be bonded to six Li atoms at most. This difference would be partly due to the atomic size effect on the packing efficiency, considering Si is much larger in size compared to O and hence able to neighbor with more Li atoms. For a quantitative understanding of the $Li_6O$ structure formation, we analyzed the underlying bonding mechanism.

Figure 4 shows the isosurfaces of maximally localized Wannier functions for the occupied 2s and 2p states of $O^{2-}$

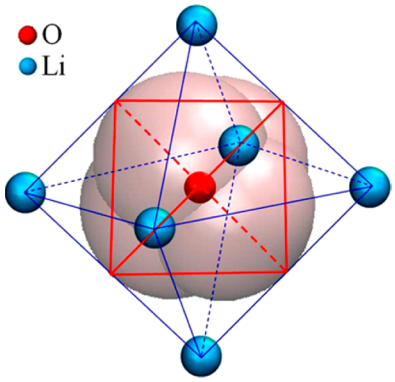


**Figure 4.** Isosurfaces (with a value of 0.08 e/Å$^3$) for the maximally localized Wannier functions calculated using the CPMD package (ref 55), which explains the dense close-packing arrangement of the $[Li_6O]^{4+}$ octahedron. The four $sp^3$-hybridized orbitals directed to the corners of a tetrahedron (in red) are surrounded by six Li cations each sitting over an edge, forming a six-fold coordinated octahedron (in blue).

in the $[Li_6O]^{4+}$ complex, which clearly exhibits the tetrahedral arrangement of four $sp^3$-hybridized orbitals to minimize electron repulsion. Surrounding the O anion, each Li cation sits over an edge of the tetrahedron, forming a six-fold coordinated $[Li_6O]^{4+}$ octahedron. The $[Li_6O]^{4+}$ octahedron likely maximizes the electrostatic attraction between the negative O and positive Li ions via a dense close-packing arrangement; the predicted Li−O distance of 1.91 ± 0.02 Å in $[Li_6O]^{4+}$ is considerably shorter than that around 2.0 Å in crystalline $Li_2O$. Such $Li_6O$ cluster formation has also been predicted in the gas phase;[56,57] however, the neutral cluster tends to be the most stable with $D_{3d}$ or $D_{2d}$ symmetry. Unlike the gas-phase cluster, the formation of $[Li_6O]^{4+}$ polycations (with $O_h$ symmetry) in highly lithiated $a$-$Li_xSiO_{1/3}$ can be possible because they are stabilized by surrounding Si anions. This is consistent with the "shell-like" model that was proposed for dilithium phosphanediide (or arsanediide), where the $[Li_6O]^{4+}$ core was found to be shelled by P (As) anions);[58−60] the experimental Li−O distances of 1.81−1.90 Å in those $[Li_6O]^{4+}$ cores are in excellent agreement with our calculation results.

The formation mechanism for the above-mentioned $[Li_6O]^{4+}$ polycations in lithiated $a$-$SiO_{1/3}$ is intriguingly different from the proposed $Li_2O$- and $Li_4SiO_4$-like cluster formation in lithiated $SiO_2$ and $Si/SiO_2$ interfaces, respecitvely.[61] These findings may suggest that the $[Li_6O]^{4+}$ formation can be rather sensitive to the Si:O atomic ratio as well as the O spatial distribution in the host (suboxide) matrix; that is, the amount of Si anions should be sufficient to stabilize $[Li_6O]^{4+}$ polycations; otherwise, $Li_2O$ and/or various lithium silicates can form, as is commonly observed during lithiation of silicon


dx.doi.org/10.1021/cm401303n | Chem. Mater. 2013, 25, 3435−3440

suboxides with high O contents ($x > 1$ in $SiO_x$).[20−29] A further investigation is underway to determine the critical O concentration, which marks the transition from a dispersed $[Li_6O]^{4+}$ complex to $Li_2O$ and/or lithium silicate formation.

**Bulk Modulus and Lithiation Energetics.** While the *a*-$SiO_{1/3}$ host undergoes considerable structural changes when alloyed with Li, we calculated the bulk modulus ($B$) of lithiated *a*-$Li_xSiO_{1/3}$ alloys to assess the lithiation effect on the mechanical properties. Here, the value of $B$ was determined by fitting the Murnaghan equation of state[62] to the corresponding energy versus volume curve. Uniform tensile and compressive stresses were imposed on the alloys to achieve ±10% volume variation.

$$E(V) = E_0 + \left(\frac{BV}{B'}\right)\left[\frac{(V_0/V)^{B'}}{B'-1} + 1\right] - \frac{V_0 B}{B'-1} \quad (2)$$

where $E$ and $E_0$ refer to the total energies of the *a*-$Li_xSiO_{1/3}$ alloy at volume $V$ and $V_0$ (equilibrium), respectively, and $B'$ is the pressure derivative of the bulk modulus.

Figure 5 shows the variations in $B$ for the *a*-$Li_xSiO_{1/3}$ and *a*-$Li_xSi$ alloys.[38] Prior to lithiation, the *a*-$SiO_{1/3}$ alloy ($B \approx 56$ GPa) is found to be considerably softer than *a*-Si ($B \approx 75$ GPa), which is mainly due to the flexible nature of the Si−O−Si units.[63] Compared to the pure Si case, the softer *a*-$SiO_{1/3}$ matrix may contribute to easier Li incorporation and better strain accommodation especially during the early stages of lithiation. With increasing Li contents, the $B$ values decrease monotonically in both alloy systems; such a softening effect is attributed to disintegration of the host matrix as well as the increasing metallic character.

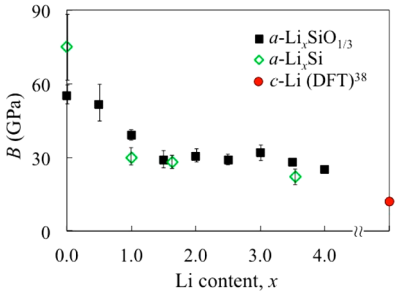


**Figure 5.** Calculated bulk moduli ($B$) for *a*-$Li_xSiO_{1/3}$ and *a*-$Li_xSi$ alloys as a function of Li content $x$.

Next, we calculated the formation energy of *a*-$Li_xSiO_{1/3}$ as a function of $x$, with respect to the *a*-$SiO_{1/3}$ host and body-centered-cubic Li (bcc-Li). The formation energy per Si atom ($E_f$) is given by

$$E_f = E_{Li_xSiO_{1/3}} - (xE_{Li} + E_{SiO_{1/3}}) \quad (3)$$

where $E_{Li_xSiO_{1/3}}$ and $E_{SiO_{1/3}}$ are the total energies per Si atom of the *a*-$Li_xSiO_{1/3}$ and *a*-$SiO_{1/3}$ systems and $E_{Li}$ is the per-atom energy of bcc-Li, which was previously calculated in ref 38 using a 16-atom supercell with a 11 × 11 × 11 mesh of $k$ points in the scheme of Monkhorst−Pack.

Figure 6a shows a comparison of the $E_f$ values of *a*-$Li_xSiO_{1/3}$ and *a*-$Li_xSi$ (which was previously calculated in ref 64); for both alloys, the $E_f$ values decrease monotonically with increasing $x$ and approach the minimum-energy "plateau" as they are fully lithiated around $x = 4$. The predicted Li storage capacity for *a*-$SiO_{1/3}$ is close to that of pure Si, which is in line with

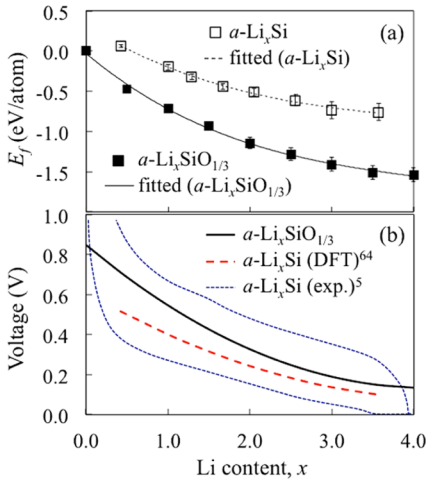


**Figure 6.** (a) Formation energies ($E_f$) for *a*-$Li_xSiO_{1/3}$ ($0 \le x \le 4$) and *a*-$Li_xSi$ ($0 \le x \le 3.57$) alloys calculated based on three different samples for each composition. (b) Voltage−composition ($V$−$x$) curve for lithiated *a*-$SiO_{1/3}$ in comparison to that of pure Si.

experimental results that show comparative first-cycle Li insertion capacities between *a*-Si films under controlled oxidation (~ 17 atom % O) and pure Si.[31] We also notice that the $E_f$ profile of *a*-$Li_xSiO_{1/3}$ is considerably lower in value compared to the *a*-$Li_xSi$ case, and exhibits a much steeper descending trend. These differences indicate that Li incorporation is energetically more favorable in *a*-$SiO_{1/3}$ compared to *a*-Si, which is reasonable considering the stronger Li−O interaction relative to the Li−Si interaction, and also the relatively easier Li accommodation in the softer *a*-$SiO_{1/3}$ matrix.

By taking the negative of the derivative of the third-order polynomial fittings according to $V = -dE_f(x)/dx$, we obtained the voltage−composition ($V$−$x$) curves for the lithiated *a*-$Li_xSiO_{1/3}$ and *a*-$Li_xSi$ systems, as shown in Figure 6b. The lithiation voltage for *a*-$SiO_{1/3}$ is predicted to be around 0.2−0.8 V, which is within the desirable range for LIB anode application but slightly higher than that of pure *a*-Si (0.1−0.5 V),[64] especially during the early stages of lithiation. The upshift in $V$ reflects the more energetically favorable incorporation of Li in *a*-$SiO_{1/3}$ (relative to *a*-Si), as discussed earlier. The results are consistent with previous experimental observations that also showed a shift toward higher Li insertion potentials for silicon suboxide based anodes with increasing O contents.[31] At very high O:Si ratios (approaching 2, for instance), the formation of stable $Li_2O$ and/or various lithium silicates during lithiation may cause a significant upshift in $V$; as a consequence, Li extraction in the following discharge cycle would be difficult, and those possibly trapped Li atoms could be partly responsible for the irreversible capacity loss. Our results clearly highlight that the capacity and cyclability can be sensitive to the local atomic arrangement of the suboxide host matrix; hence, fine-tuning of the concentration and spatial distribution of O atoms would be essential in order to maximize the performance of silicon suboxide based anodes.

## 4. CONCLUSION

DFT calculations were performed to examine the lithiation behavior of the *a*-$SiO_{1/3}$ suboxide, specifically regarding structural evolution, bonding mechanism, bulk modulus variation, and lithiation energetics. Our calculations show that both Si and O are active toward Li; with increasing Li contents,


dx.doi.org/10.1021/cm401303n | Chem. Mater. 2013, 25, 3435−3440

the charge states of Li and O are predicted to remain nearly constant around 0.8+ to 0.9+ and 1.6− to 1.8−, respectively, while the Si charge state varies from 0.6+ to 3.5−, depending on the numbers of neighboring Li and/or O atoms. Because of the electrostatic interaction between the cationic Li and anionic Si/O atoms, Si and O atoms are surrounded by Li atoms; with lithiation, Si−Li CN is found to monotonically increase up to $CN_{Si-Li} \approx 10$ when fully lithiated, whereas $CN_{O-Li}$ tends to saturate at 6, far before full lithiation. Our electronic structure analysis clearly demonstrates the tetrahedral arrangement of the four $sp^3$-hybridized orbitals of an isolated $O^{2-}$ anion to minimize electron repulsion; the surrounding Li cations sit over the edges of the tetrahedron, forming a six-fold coordinated $[Li_6O]^{4+}$ octahedron with $O_h$ symmetry. With increasing Li content $x$, the $a$-$Li_xSiO_{1/3}$ matrix gradually disintegrates and softens, as indicated by the substantial decrease in the bulk modulus. Furthermore, the lithiation voltage profiles demonstrate a likely dependency of the capacity and cyclability on the O content and distribution. While the soft $a$-$SiO_{1/3}$ matrix of a low O content may facilitate Li incorporation, thus delivering a competitive capacity relative to pure Si, if the O:Si ratio was further increased beyond a certain threshold, the formation of stable $Li_2O$ and/or various lithium silicates may result in irreversible capacity loss and thus compromise the benefits of using silicon suboxides as the anode material. The present work sheds light on the importance of the O concentration and spatial distribution, and high-performance Si suboxide anodes may be designed via fine-tuning of the oxidation conditions.

## AUTHOR INFORMATION


### Corresponding Author

*E-mail: gshwang@che.utexas.edu.


### Notes

The authors declare no competing financial interest.

## ACKNOWLEDGMENTS

This work was partially supported by the National Science Foundation (Grant CBET-0933557), the Welch Foundation (Grant F-1535), and SK Innovation Co., Ltd. We thank the Texas Advanced Computing Center for use of their computing resources.

## REFERENCES


(1) Winter, M.; Besenhard, J. O. *Electrochim. Acta* **1999**, *45*, 31.
(2) Sharma, R. A.; Seefurth, R. N. *J. Electrochem. Soc.* **1976**, *123*, 1763.
(3) Boukamp, B. A.; Lesh, G. C.; Huggins, R. A. *J. Electrochem. Soc.* **1981**, *128*, 725.
(4) Obrovac, M. N.; Christensen, J. *Electrochem. Solid-State Lett.* **2004**, *5*, A93.
(5) Hatchard, T. D.; Dahn, J. R. *J. Electrochem. Soc.* **2004**, *151*, A838.
(6) Beaulieu, L. Y.; Hewitt, K. C.; Turner, R. L.; Bonakdarpour, A.; Abdo, A. A.; Christensen, L.; Eberman, K. W.; Krause, L. J.; Dahn, J. R. *J. Electrochem. Soc.* **2003**, *150*, A149.
(7) Mao, O.; Turner, R. L.; Courtney, I. A.; Fredericksen, B. D.; Buckett, M. I.; Krause, L. J.; Dahn, J. R. *Electrochem. Solid-State Lett.* **1999**, *2*, 3.
(8) Fleischauer, M. D.; Topple, J. M.; Dahn, J. R. *Electrochem. Solid-State Lett.* **2005**, *8*, A137.
(9) Gao, B.; Sinha, S.; Fleming, L.; Zhou, O. *Adv. Mater.* **2001**, *31*, 816.
(10) Graetz, J.; Ahn, C. C.; Yazami, R.; Fultz, B. *Electrochem. Solid-State Lett.* **2003**, *6*, A194.
(11) Chan, C. K.; Peng, H.; Liu, G.; McIlwrath, K.; Zhang, X. F.; Huggins, R. A.; Cui, Y. *Nat. Nanotechnol.* **2008**, *3*, 31.
(12) Feng, X.; Yang, J.; Gao, P.; Wang, J.; Nuli, Y. *RSC Adv.* **2012**, *2*, 5701.
(13) Wang, C. M.; Li, X.; Wang, Z.; Xu, W.; Liu, J.; Gao, F.; Kovarik, L.; Zhang, J.-G.; Howe, J.; Burton, D. J.; Liu, Z.; Xiao, X.; Thevuthasan, S.; Baer, D. R. *Nano Lett.* **2012**, *12*, 1624.
(14) Howe, J. Y.; Burton, D. J.; Qi, Y.; Meyer, H. M., III; Nazri, M.; Nazri, G. A.; Palmer, A. C.; Lake, P. D. *J. Power Sources* **2013**, *221*, 455.
(15) Lai, J.; Guo, H.; Wang, Z.; Li, X.; Zhang, X.; Wu, F.; Yue, P. *J. Alloys Compd.* **2012**, *530*, 30.
(16) Song, T.; Lee, D. H.; Kwon, M. S.; Choi, J. M.; Han, H.; Doo, S. G.; Chang, H.; Park, W. I.; Sigmund, W.; Kim, H.; Paik, U. *J. Mater. Chem.* **2011**, *21*, 12619.
(17) Li, Y.; Guo, B.; Ji, L.; Lin, Z.; Xu, G.; Liang, Y.; Zhang, S.; Toprakci, O.; Hu, Y.; Alcoutlabi, M.; Zhang, X. *Carbon* **2013**, *51*, 185.
(18) Wang, J. W.; Liu, X. H.; Zhao, K.; Palmer, A.; Patten, E.; Burton, D.; Mao, S. X.; Suo, Z.; Huang, J. Y. *ACS Nano* **2012**, *6*, 9158.
(19) Klankowski, S. A.; Rojeski, R. A.; Cruden, B. A.; Liu, J.; Wu, J.; Li, J. *J. Mater. Chem. A* **2013**, *1*, 1055.
(20) Kim, T.; Park, S.; Oh, S. M. *J. Electrochem. Soc.* **2007**, *154*, A1112.
(21) Song, K.; Yoo, S.; Kang, K.; Heo, H.; Kang, Y.-M.; Jo, M.-H. *J. Power Sources* **2013**, *229*, 229.
(22) Hwa, Y.; Park, C.-M.; Sohn, H.-J. *J. Power Sources* **2013**, *222*, 129.
(23) Yamamura, H.; Nobuhara, K.; Nakanishi, S.; Iba, H.; Okada, S. *J. Ceram. Soc. Jpn.* **2011**, *119*, 855.
(24) Yang, J.; Takeda, Y.; Imanishi, N.; Capiglia, C.; Xie, J. Y.; Yamamoto, O. *Solid State Ionics* **2002**, *152−153*, 125.
(25) Nagao, Y.; Sakaguchi, H.; Konda, H.; Fukunaga, T.; Esaka, T. *J. Electrochem. Soc.* **2004**, *151*, A1572.
(26) Chang, W.-S.; Park, C.-M.; Kim, J.-H.; Kim, Y.-U.; Jeong, G.; Sohn, H.-J. *Energy Environ. Sci.* **2012**, *5*, 6895.
(27) Guo, H.; Mao, R.; Yang, X.; Chen, J. *Electrochim. Acta* **2012**, *74*, 271.
(28) Kim, J.-H.; Park, C.-M.; Kim, H.; Kim, Y.-J.; Sohn, H.-J. *J. Electroanal. Chem.* **2011**, *661*, 245.
(29) Miyachi, M.; Yamamoto, H.; Kawai, H.; Ohta, T.; Shirakata, M. *J. Electrochem. Soc.* **2005**, *152*, A2089.
(30) Kim, K.; Park, J.-H.; Doo, S.-G.; Kim, T. *Thin Solid Films* **2010**, *518*, 6547.
(31) Abel, P. R.; Lin, Y.-M.; Celio, H.; Heller, A.; Mullins, C. B. *ACS Nano* **2012**, *6*, 2506.
(32) Iacona, F.; Bongiorno, C.; Spinella, C.; Boninelli, S.; Priolo, F. *J. Appl. Phys. Lett.* **2004**, *95*, 3723.
(33) Wang, Y. Q.; Smirani, R.; Ross, G. G. *J. Cryst. Growth* **2006**, *294*, 486.
(34) Park, C.-M.; Choi, W.; Hwa, Y.; Kim, J.-H.; Jeong, G.; Sohn, H.-J. *J. Mater. Chem.* **2010**, *20*, 4858.
(35) Mamiya, M.; Takei, H.; Kikuchi, M.; Uyeda, C. *J. Cryst. Growth* **2001**, *229*, 457.
(36) Mamiya, M.; Kikuchi, M.; Takei, H. *J. Cryst. Growth* **2002**, *137*, 1909.
(37) Lee, S.-H.; Hwang, G. S. *J. Chem. Phys.* **2007**, *127*, 224710.
(38) Kim, H.; Chou, C.-Y.; Ekerdt, J. G.; Hwang, G. S. *J. Phys. Chem. C* **2012**, *115*, 2514.
(39) Yu, D.; Lee, S.; Hwang, G. S. *J. Appl. Phys.* **2007**, *102*, 084309.
(40) Yu, D.; Hwang, G. S. *Phys. Rev. B* **2005**, *72*, 205204.
(41) Yu, D.; Kirichenko, T. A.; Banerjee, S.; Hwang, G. S. *Phys. Rev. B* **2005**, *72*, 205204.
(42) Blochl, P. E. *Phys. Rev. B* **1994**, *50*, 17953.
(43) Kresse, G.; Hafner, J. *Phys. Rev. B* **1993**, *47*, 558.
(44) Kresse, G.; Furthmuller, J. *Comput. Mater. Sci.* **1996**, *6*, 15.
(45) Kresse, G.; Furthmuller, J. *Phys. Rev. B* **1996**, *54*, 11169.
(46) Monkhorst, H. J.; Pack, J. D. *Phys. Rev. B* **1976**, *13*, 5188.
(47) Allen, M.; Tildesley, D. *Computer Simulation of Liquids*; Oxford University Press: New York, 1987; p 54.
(48) Plans, J.; Diaz, G.; Martinez, E.; Yndurain, F. *Phys. Rev. B* **1987**, *35* (2), 788.

(49) Martinez, E.; Plans, J.; Yndurain, F. *Phys. Rev. B* **1987**, *36* (15), 8043.
(50) Islam, M. M.; Bredow, T. *J. Phys. Chem. C* **2009**, *113*, 673.
(51) De Jong, B. H. W. S.; Supèr, H. T.; Spek, A. L.; Veldman, N.; Hachtegaal, G.; Fischer, J. C. *Acta Crystallogr.* **1998**, *B54*, 568.
(52) Tranqui, D.; Shannon, R. D.; Chen, H.-Y. *Acta Crystallogr.* **1979**, *B35*, 2479.
(53) Henkelman, G.; Arnaldsson, A.; Jonsson, H. *Comput. Mater. Sci.* **2006**, *36*, 354.
(54) Chan, M. K. Y.; Wolverton, C.; Greeley, J. P. *J. Am. Chem. Soc.* **2012**, *134*, 14362.
(55) Wu, C. H.; Kudo, H.; Ihle, H. R. *J. Chem. Phys.* **1979**, *70*, 1815.
(56) Wu, C. H. *Chem. Phys. Lett.* **1987**, *139*, 357.
(57) Zheng, X.; Wang, Z.; Feng, J.; Tang, A. *THEOCHEM* **1999**, *469*, 115.
(58) Chen, W.; Li, Z.-R.; Wu, D.; Li, Y.; Sun, C.-C. *J. Chem. Phys.* **2005**, *123*, 164306.
(59) Driess, M.; Pritzkow, H.; Martin, S.; Rell, S.; Fenske, D.; Baum, G. *Angew. Chem., Int. Ed. Engl.* **1996**, *35*, 986.
(60) Centeno, J.; Contreras, R.; Fuentealba, R. *J. Phys. Chem. A* **2009**, *113*, 13451.
(61) Ban, C.; Kappes, B. B.; Qiang, X.; Engtrakul, C.; Ciobanu, C. V.; Dillon, A. C.; Zhao, Y. *Appl. Phys. Lett.* **2012**, *100*, 243905.
(62) Murnaghan, F. D. *Proc. Natl. Acad. Sci. U. S. A.* **1994**, *30*, 244.
(63) Lee, S.; Bondi, R. J.; Hwang, G. S. *Phys. Rev. B* **2011**, *84*, 045202.
(64) Chou, C.-Y.; Hwang, G. S. *Surf. Sci.* **2013**, *612*, 16.